High pressure measurement of the uniaxial stress of host layers on intercalants and staging transformation of intercalation compounds



2002 J. Phys.: Condens. Matter 14 11687

(http://iopscience.iop.org/0953-8984/14/45/311)

INSTITUTE OF PHYSICS PUBLISHING JOURNAL OF PHYSICS: CONDENSED MATTER

J. Phys.: Condens. Matter **14** (2002) 11687–11700 PII: S0953-8984(02)36202-7

# High pressure measurement of the uniaxial stress of host layers on intercalants and staging transformation of intercalation compounds

**Ta-Ryeong Park**[1,3], **Tae Yang Park**[1], **Hyungrok Kim**[2] **and Peera Min**[2]

[1] Department of Physics, Hoseo University, Asan, Choongnam 336-795, Korea
[2] Chemical Technology Research Division, Korea Research Institute of Chemical Technology, Taejon 305-606, Korea

E-mail: trpark@dogsuri.hoseo.ac.kr

Received 24 April 2002, in final form 15 August 2002
Published 1 November 2002
Online at stacks.iop.org/JPhysCM/14/11687

**Abstract**

A layered double-hydroxide intercalation compound was synthesized to measure the uniaxial stress the host layers exert on the intercalants. To measure the uniaxial stress, we employed the photoluminescence (PL) from the intercalated species, the Sm ion complex, as it is sensitive to the deformation of the intercalants. Of the many PL peaks the Sm ion complex produces, the one that is independent of the counter-cation environment was chosen for the measurement since the Sm ion complexes are placed under a different electrostatic environment after intercalation. The peak position of the PL was redshifted linearly with increasing hydrostatic pressure on the intercalated sample. Using this pressure-induced redshifting rate and the PL difference at ambient pressure between the pre-intercalation and the intercalated ions, we found that, in the absence of external pressure, the uniaxial stress exerted on the samarium ion complexes by the host layers was about 13.9 GPa at room temperature. Time-resolved PL data also supported this observation. The uniaxial stress showed a large variation with temperature, decreasing to 7.6 GPa at 28 K. This very unusual behaviour implies that staging transformation towards a higher degree occurs at low temperatures. It was also observed that the redshift rate of the PL was slowed down at higher temperatures. This effect is equivalent to the decreased deformation rate of the intercalants at higher temperatures and is explained by the pressure-induced staging transition.

[3] Author to whom any correspondence should be addressed.

  

## 1. Introduction

It is well known that layered solids like graphite [1], layered alumino-silicate clay [2, 3] and layered double hydroxides (LDHs) [4] form intercalation compounds [1, 5]. In the intercalation compounds that are prepared by ion-exchange methods, the chemical composition and structure of the intercalated species remain unchanged during the intercalation process [6]. Therefore the intercalation compounds are useful for investigating the properties of chemical species contained in restricted space. The flexibility of host layers of the layered solids allows them to pucker around the intercalants and this aspect has been experimentally [7, 8] confirmed. In addition to the usual Coulomb interaction, the intercalants elastically interact either repulsively or attractively due to the elastic deformation of the host layers. This elastic interaction between the intercalants is one of the primary factors that are responsible for the staging phenomenon [1, 5]. The finite rigidities of the intercalants will make them deformed in the gallery and this will subsequently affect the elastic interaction [9, 10] between them.

While the elastic deformation of the host layers has been investigated by many workers [11–18], the deformation of the intercalants has been largely neglected. As alluded to above, consideration of the deformation of both the intercalants and the host layers is necessary in the structural investigation of the intercalation compounds. It will also be necessary for utilization of the physical properties of the intercalants confined in restricted space. In this paper, we report the photoluminescence (PL) of the negatively charged samarium ion complexes that were intercalated into the LDH. By comparing the PL of the samarium ion complex after the intercalation with that before the intercalation, we measure the uniaxial stress that the host layers exert on the samarium ion complexes. Since the thin film of intercalated LDH sample with a thickness of $\sim$100 $\mu$m shows partial transparency with visible light, it is evident that the information obtained by the PL represents the properties of the bulk, not of the surface. (The samples we used had typical size much smaller than 100 $\mu$m.)

Application of hydrostatic pressure causes reduction of the lattice spacing while preserving the crystal symmetry if the structural phase transition does not occur. This corresponds to the case of the samarium ion complexes under hydrostatic pressure when they are not intercalated. However, when they are in the gallery space, they are subjected to uniaxial stress along the $c$-axis even though the entire intercalation compound is under hydrostatic pressure. This behaviour is due to the fact that the pressure-transmitting medium can act only on the host layers. (Notice that in order to directly pressurize the intercalants, enough of the pressure-transmitting medium should be inserted into the gallery space. In the present case, we used a mixture of methyl alcohol and ethyl alcohol as the pressure-transmitting fluid and their molecular dimensions are compatible with insertion into the gallery space. Also, their electrical neutrality will allow some to be inserted into the gallery when external pressure exists. However, in the restricted space between the host layers whose size along the $c$-axis direction is comparable to that of molecules, the alcohol molecules will exist independently or in the form of aggregates of only a few. In addition to this, due to the energy cost for the movement of the alcohol molecules, it is very improbable that the alcohol molecules will mediate the hydrostatic pressure in the nearly two-dimensional gallery space.)

To the authors' knowledge, to date there has been no pressure-related research regarding the deformation of the intercalants between the host layers, although pressure-induced stage transformation [19] in the GIC was studied with hydrostatic pressure experiment. In [20, 21], chromium ion complexes and cobalt ion complexes were co-intercalated into the fluorohectorite to form ternary intercalation compounds. By changing the relative amount of the cobalt and chromium complexes, the average gallery spacing was varied and the resulting change in the PL was observed. The PL lifetime of the chromium depended on the gallery spacing. It was

assumed that the change in the uniaxial stress on the chromium complex was responsible for the change in the PL lifetime. Therefore, one of the purposes of the present paper is to prove that assumption via pressure experiments.

## 2. Experimental details

As the excitation sources for the PL, we used the 488 nm of a continuous wave (CW) argon-ion laser and the pulsed 532 nm of a frequency doubled Nd:YAG laser. PL was collected in a back-scattering configuration and was dispersed by a 50 cm single-grating monochromator after passing through a holographic notch filter to remove elastically scattered laser light. Correction for the spectral response of the equipment was not performed. A cryogenically cooled charge-coupled device was employed to record the CW line shapes of the PL. The time-resolved PL was obtained employing the well known 'time-correlated single-photon counting method' [22] and using a thermoelectrically cooled photo-multiplier tube and the ancillary electronics. Since the pulse repetition rate of the 532 nm laser was about 12 kHz, the photon counting rate was kept below 1 kHz when collecting the time-resolved signal.

A Merrill–Bessett type diamond-anvil cell (DAC) was employed to generate the hydrostatic pressure using a 4:1 mixture of methanol and ethanol as the pressure-transmitting medium. The sample chamber was made of a stainless steel gasket whose hole diameter was 0.2–0.3 mm. Pressure was monitored by measuring the $R_1$-line PL position (694.24 nm at 25 °C) of a ruby chip that was put into the gasket hole with the sample [23]. The highest pressure we applied in this experiment was 7.6 GPa. A closed-cycle helium cryostat was used to lower the temperature down to ∼28 K. Since isolation of the cold head vibration was not necessary, the DAC was directly attached to the cold finger. To measure temperature precisely, a temperature sensor was attached to the DAC. The cold head of the cryostat was mounted on a triple-axis micro-positioning device for precise alignment of the DAC.

Sm ion compounds $Na_9(SmW_{10}O_{36})$, $Cs_9(SmW_{10}O_{36})$, $(HN(n\text{-butyl})_3)_9(SmW_{10}O_{36})$ and $K_{11}[Sm(PW_{11}O_{39})_2]$ were prepared following the literature method [24]. $Na_9(SmW_{10}O_{36})$ and $Cs_9(SmW_{10}O_{36})$ were re-crystallized in water–alcohol solvent. $(HN(n\text{-butyl})_3)_9(SmW_{10}O_{36})$ was purified by repeated precipitation from heptane solution. The $(SmW_{10}O_{36})^{9-}$ ion intercalated compound, $SmW_{10}O_{36}$–LDH, was prepared by the ion exchange method. $OH^-$ ion in OH-LDH which can be obtained via thermal treatment and re-hydration of $CO_3$-LDH was exchanged with $(SmW_{10}O_{36})^{9-}$ ion using an excess amount of $Na_9(SmW_{10}O_{36})$ in aqueous medium of pH 8 under $N_2$ flow. The Mg to Al mole ratio in the starting $CO_3$-LDH was 2 [4]. The ion exchange reaction was continued until no corresponding x-ray diffraction (XRD) peak of $CO_3$-LDH was observed. The separated $SmW_{10}O_{36}$–LDH was washed with distilled water and dried for 24 h at 100 °C. The chemical compositions of samples were confirmed using the atomic absorption spectroscopy (AAS) method and the x-ray photoelectron spectroscopy (XPS) method.

The good efficiency of intercalation was confirmed by the PL of the intercalated LDH: as will be seen later in figure 3, the PL of the intercalated LDH, $SmW_{10}O_{36}$–LDH, did not contain any PL component of the unintercalated samarium ion complexes, $Cs_9(SmW_{10}O_{36})$.

## 3. Results and discussion

### *3.1. Measurement of uniaxial stress on intercalants*

In order to investigate the effect of intercalation on the deformation of the intercalants, we synthesized single-phase $SmW_{10}O_{36}$–LDH intercalation compounds where $SmW_{10}O_{36}$ is the

intercalated species and LDH is the host material. Samarium complex was chosen as the intercalating species because it produces intense PL even at room temperature. When the samarium complexes are placed in the gallery space between the host layers, they undergo deformation due to the uniaxial stress exerted by the bounding host layers. Thus even in the absence of external pressure, the PL of the intercalated species differs from that of the pre-intercalation one ($Cs_9(SmW_{10}O_{36})$ or $Na_9(SmW_{10}O_{36})$). This leads to the expectation that the uniaxial stress can be measured by the change in the PL.

The negatively charged samarium complexes can be intercalated into the gallery spaces of the LDH since the latter are positively charged. The area charge density of the LDH host layers is $e^+/40$ Å$^2$ which is about 2.5 times as large as that of 2:1 layered silicate clay. This means that with LDH one has the advantage of working with higher density of intercalants and consequently stronger PL. The LDH is also well suited for intercalating large luminescent complexes because upon intercalation it expands only in the *c*-axis direction without other side effects. The transverse rigidity of the LDH is larger than that of graphite, but smaller than that of the 2:1 layered silicate clay. This is due to the fact that the number of atomic layers comprising the host layer of the LDH, graphite and the 2:1 layered silicate clay is three, one and seven, respectively.

Figure 1(a) shows the schematic view of the intercalated $SmW_{10}O_{36}$–LDH where $(SmW_{10}O_{36})^{9-}$ ion complexes are located between the host layers. Figure 1(b) shows the schematic structure of the LDH host layers flanking anions (designated by $A^-$) and water molecules. The central atomic layer of the host layer is composed of only $Mg^{2+}$ (designated by M(II)) and $Al^{3+}$ (designated by M(III)) ions with 2:1 mole ratio. Each of these ions is connected to six $OH^-$ ions in the upper and lower bounding atomic layers. Therefore the host layer can be viewed as being composed of connected octahedrons whose vertices are $OH^-$ ions. In the centre of these octahedrons are located either $Mg^{2+}$ or $Al^{3+}$ ions that are responsible for the positive charge of the LDH host layers. The thickness of the host layer is about 0.45 nm.

The negative ions (designated by $A^-$ in figure 1(b)) located in between the host layers ensure the overall electrical neutrality and can be exchanged with many different kinds of other negative ion. The ions of large negative charges and appropriate physical size are particularly suitable for the quantitative ion exchange reaction [4]. The samarium ion complex $(SmW_{10}O_{36})^{9-}$ which possesses large negative charge of $-9e$ was useful for ion exchange reaction and XRD [25] and chemical analysis of $SmW_{10}O_{36}$–LDH show that the $(SmW_{10}O_{36})^{9-}$ ion has been well intercalated into the gallery space of the LDH host layers. From the XRD analysis it was found that the *c*-axis repeat distance, $d_{001}$, of $SmW_{10}O_{36}$–LDH is 1.14 nm, from which we infer that the pillaring height of the samarium complex in the gallery space is $1.14 - 0.45$ nm $= 0.69$ nm.

Figure 1(c) represents schematically the structure of the samarium ion complex $(SmW_{10}O_{36})^{9-}$. It has been proposed by the structural analysis of iso-structural $(CeW_{10}O_{36})^{8-}$ [26]. The central $Sm^{3+}$ ion achieves eightfold coordination by the attachment to oxo ligands of two $W_5O_{18}$ groups that have a staggered arrangement close to $C_{4v}$ symmetry.

The molecular dimensions of the $(SmW_{10}O_{36})^{9-}$ ion of figure 1(c) can be estimated to be at least 1.6 nm and about 0.8 nm along the long and the short axis, respectively, by applying those of iso-structual $(CeW_{10}O_{36})^{8-}$ ion species [26]. The long axis of the $(SmW_{10}O_{36})^{9-}$ ion in $SmW_{10}O_{36}$–LDH should be parallel to the layers since 0.69 nm of gallery height is compatible with 0.8 nm of the estimated short axis dimension.

Chemical analysis for $SmW_{10}O_{36}$–LDH showed that the Mg to Al mole ratio was 2.0 and the Sm to W mole ratio was the same as in $Na_9(SmW_{10}O_{36})$, which means that the $(SmW_{10}O_{36})^{9-}$ ion moiety in the LDH gallery is unchanged and the ideal composition of $Mg_2Al(OH)_6(SmW_{10}O_{36})_{1/9}$ can be applied for the $SmW_{10}O_{36}$–LDH sample.

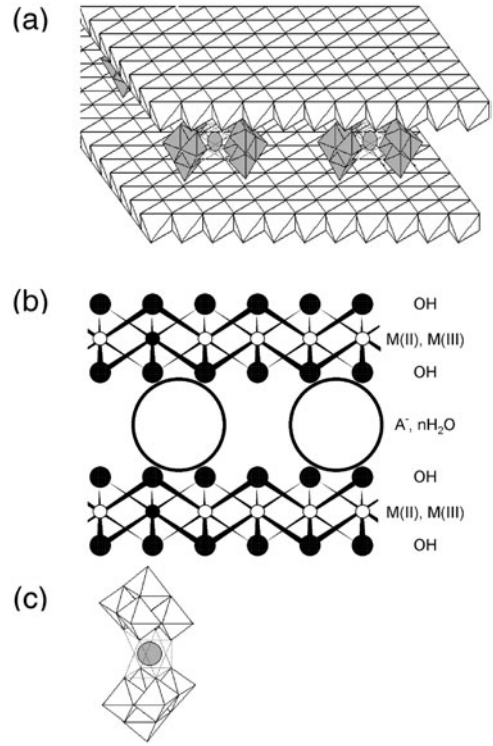


**Figure 1.** (a) Schematic view of the structure of the LDH intercalation compound. Shaded parts represent the Sm ion complexes, the intercalants. (b) Lateral view of the LDH intercalation compound. The top and bottom layers are the host layers and the large circles in between them are negative ions ($A^-$) and water molecules ($nH_2O$). M(II) and M(III) represent $Mg^{2+}$ and $Al^{3+}$ ions, respectively. (c) Schematic drawing of the samarium ion complex $(SmW_{10}O_{36})^{9-}$. The central shaded circle is the $Sm^{3+}$ ion, at the vertices of the small octahedrons are the oxygen atoms and the W atoms are located at the centre of the small octahedrons. Five small octahedrons compose a large lacunary octahedron (one small octahedron is vacant) and the two lacunary octahedrons are in a twisted configuration with respect to each other.

Figure 2(a) shows the PL from the $Na_9(SmW_{10}O_{36})$ compound at room temperature at ambient pressure, excited by the 488 nm laser light. The PL is distributed over a wide range covering from ∼550 to ∼750 nm. These sharp PL peaks originate from the intra-4f → 4f transition within the $4f^5$ of $Sm^{3+}$ ions where spin–orbit interaction plays a role in determining the $4f^5$ states. Comparison of our data with those of [27] reveals that the group of PL peaks around 560 nm is due to the transition $^4G_{5/2} \rightarrow {}^6H_{5/2}$, that around 600 nm is due to $^4G_{5/2} \rightarrow {}^6H_{7/2}$ and that around 650 nm is due to $^4G_{5/2} \rightarrow {}^6H_{9/2}$. (Notice that in [27] PL in the range longer than 750 nm was observed, but we did not make observations in that range.) The number of energy states and their energy values are determined by the symmetry of the site where the samarium ion is located. The energy levels of the $Sm^{3+}$ ions are split by the ligand field surrounding the $Sm^{3+}$ ions. This is responsible for the many peaks in each PL group of figure 2(a) and hence the complexity of the PL line shape.

Figure 2(b) shows the room temperature PL of the intercalation compound $SmW_{10}O_{36}$–LDH under ambient pressure. The lower curve represents a typical PL lineshape of the intercalated LDH excited by 488 nm laser light while the upper one represents a typical one excited by 532 nm. With 532 nm excitation the PL lineshape looks similar, but displaced

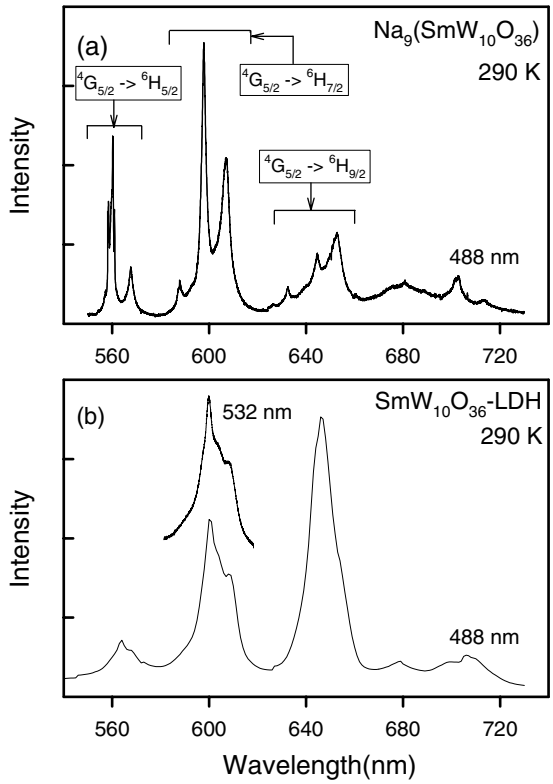


**Figure 2.** Room temperature PL from (a) $Na_9(SmW_{10}O_{36})$ and (b) $SmW_{10}O_{36}$–LDH. The PL peaks arise from the intra-$4f^5$ transition of $Sm^{3+}$ ions in both cases. The PL lineshape shown in (a) and the lower curve of (b) were obtained with 488 nm excitation while the upper curve of (b) was obtained with 532 nm excitation.

along the vertical direction due to the strong broad luminescence from the LDH host layers. (Notice that when $Na_9(SmW_{10}O_{36})$ or $Cs_9(SmW_{10}O_{36})$ is ion exchanged with LDH to form intercalation compounds, the cation $Na^+$ or $Cs^-$ does not move into the gallery.) Figure 2(b) differs from figure 2(a): after intercalation the positions of small peaks were shifted and, in particular, many sharp peaks disappeared. In the work of Yoo *et al* [28] it was reported that sharp PL peaks of $Sm^{2+}$ ions doped in $SrF_2$ diminish with increasing hydrostatic pressure and they almost disappear in the pressure range above 4 GPa. We also measured the PL of $Cs_9(SmW_{10}O_{36})$ salt at 28 K under 0 GPa. Compared to the data at room temperature, the number of sharp peaks increased significantly at 28 K. However, applying hydrostatic pressure of 6 GPa at the same temperature removed many sharp peaks. Correlating these observations with the data shown in figure 2, we may tentatively think that the host layers of $SmW_{10}O_{36}$–LDH are exerting pressure of several GPa on the samarium intercalants in the absence of external pressure.

This observation appears to be inconsistent with the symmetry consideration. First, the number of PL peaks would remain invariant with the application of hydrostatic pressure as it preserves the symmetry. Second, application of uniaxial stress lowers the symmetry of the samarium ion complex and this leads to an increased number of transitions and thus would lead to an even greater number of PL peaks. This contradiction can be well understood by considering a configuration coordinate diagram. Increasing the hydrostatic pressure or the

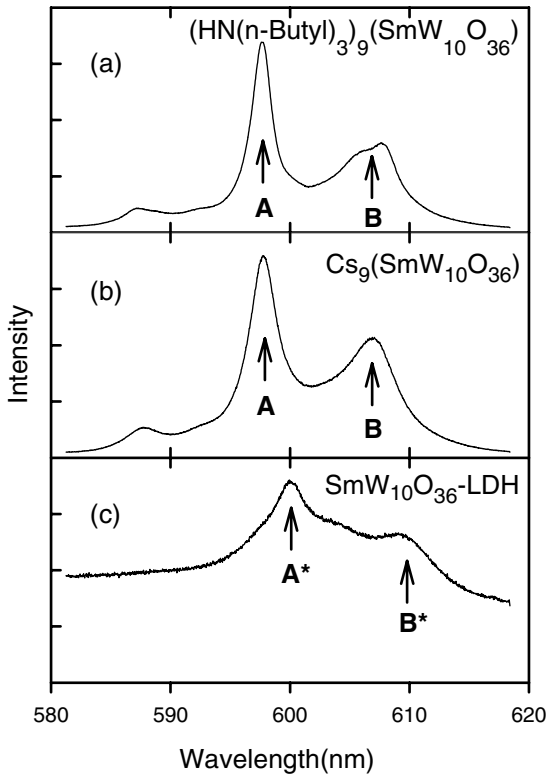


**Figure 3.** Room temperature PL from (a) (HN($n$-butyl)$_3$)$_9$($SmW_{10}O_{36}$), (b)$Cs_9$($SmW_{10}O_{36}$) and (c) $SmW_{10}O_{36}$–LDH. The chemical formula of $n$-butyl is $CH_3$–$CH_2$–$CH_2$–$CH_2$–. While peak position A is left invariant in changing cation environment from (a) to (b), the shape of B changes. Thus the shift of peak A to A* is caused only by the uniaxial stress. But both the change in the positive charge distribution and the uniaxial stress contribute to the shift from B to B*.

uniaxial stress will lead to an increase in the strength of interaction between the electronic state and the environment (phonon). In particular, the coupling strength of the electronic excited state with the environment will be more enhanced than that of the electronic ground state. Therefore, under high pressure, the horizontal shift between the minima of the excited and the ground state is enhanced in the configuration coordinate diagram. Thus when the electrons de-excite from the excited state to a group of ground states, the latter is in the region of steeper slopes and accordingly has larger chance of mutual overlap that has the effect of reducing the number of PL peaks and broadening the peaks.

With laser excitation of 532 nm, a broad and strong background PL is observed (upper curve of figure 2(b)). This background PL originates from the LDH host layers, which was confirmed with the pristine LDH sample. (The 532 nm was much more effective than the 488 nm in producing this background PL, but much less effective in producing the PL from samarium ions.)

Figure 3 compares the PL around 600 nm from three samples that were excited by 488 nm. The PL from (HN($n$-butyl)$_3$)$_9$($SmW_{10}O_{36}$), $Cs_9$($SmW_{10}O_{36}$) and $SmW_{10}O_{36}$–LDH is shown in figures 3(a), (b) and (c), respectively. (Notice that both $Cs_9$($SmW_{10}O_{36}$) and $Na_9$($SmW_{10}O_{36}$) produce the same PL lineshapes in the region between ∼550 and ∼750 nm.) The chemical formula of $n$-butyl is $CH_3$–$CH_2$–$CH_2$–$CH_2$–, from which we see that the cation size of the

sample in figure 3(a) is much larger than that in figure 3(b). Comparing figures 3(a) and (b) we see that while the position of peak A centring at 597.89 nm is the same in both cases, the shape and position of peak B are different (or peak B might be split in figure 3(a)). This is indicative of the fact that while peak A is unaffected by the change in the cation environment surrounding the samarium complex, peak B is slightly affected. (On the other hand, we observed that $K_{11}[Sm(PW_{11}O_{39})_2]$ shows a PL that is markedly different from that of $Na_9(SmW_{10}O_{36})$, implying that small variation of ligand environment strongly alters the PL of the $Sm^{3+}$ ion even though the same coordination number of eight is maintained.)

The PL of $SmW_{10}O_{36}$–LDH in figure 3(c) is redshifted and broadened relative to those in figures 3(a) and (b). Upon intercalation, samarium complexes experience two kinds of change: first, cation changes from $Cs^+$ or $Na^+$ to positively charged LDH host layers; second, samarium ion complexes are deformed by the uniaxial stress exerted by the host layers. Therefore, considering the result of figures 3(a) and (b), the reason for the redshift from A to A* in figure 3 lies solely in the deformation of the samarium ion complexes. However, peak B* in figure 3(c) is redshifted due to the influence of both the change in the cation environment and of the deformation of the samarium ion complexes. It then follows that between peaks A* and B* only A* is available for measuring the uniaxial stress.

Figure 4 shows the hydrostatic pressure dependence of the PL lineshapes at room temperature around 600 nm. For the sake of comparison the lineshapes were normalized and shifted along the vertical direction. Figure 4(a) shows the PL of $Cs_9(SmW_{10}O_{36})$ and figure 4(b) shows the PL of $SmW_{10}O_{36}$–LDH. In both cases the peak position redshifts with increasing hydrostatic pressure, which is in agreement with the report of [28] where the PL of the $Sm^{2+}$ ion was shown to be redshifting with pressure. (In the case of $Sm^{2+}$ in [28], both the broad PL due to the 5d $\rightarrow$ 4f transition and the one due to the 4f $\rightarrow$ 4f transition redshifted with increasing pressure.)

Pressure-dependent positions of the PL peaks A and A*, indicated with arrows in figure 4, are displayed in figure 5. Filled circles represent positions of peak A and empty circles A*. Solid lines are the fitting of the experimental data with straight lines. (Here, the peak positions of A and A* were obtained by fitting combinations of six and five Lorentzian curves to the PL lineshapes in figures 4(a) and (b), respectively. This choice of the number of Lorentzian curves in the combination becomes evident with the PL lineshapes at 28 K.)

From the fitting, we find that the wavelength change rates (pressure coefficient) for peaks A and A* at room temperature are given by

$$\left(\frac{\mathrm{d}\lambda}{\mathrm{d}P}\right)_A = (2.88 \pm 0.17)\ \text{Å GPa}^{-1},$$

$$\left(\frac{\mathrm{d}\lambda}{\mathrm{d}P}\right)_{A^*} = (1.63 \pm 0.16)\ \text{Å GPa}^{-1}.$$

The difference of pressure coefficient between $Cs_9(SmW_{10}O_{36})$ and $SmW_{10}O_{36}$–LDH in figure 5 may be accounted for by the difference of effects on two materials the same pressure generates. As hydrostatic pressure increases, $Cs_9(SmW_{10}O_{36})$ contracts while preserving crystal symmetry, but the Sm ion complex, $(SmW_{10}O_{36})^{9-}$, in $SmW_{10}O_{36}$–LDH deforms in a different way for it is subjected to uniaxial stress in the gallery space.

As we have seen in figure 4, the position of peak A of the samarium ion complex is independent of the cation environment. Thus, without the deformation due to the uniaxial stress, the samarium ion complex would exhibit the same PL even in the gallery space where the positive charge distribution surrounding the samarium ion complex is very different from that of the salt. Thus in the absence of external pressure, the difference of the PL peaks A and A* from the $Sm^{3+}$ ions in two materials, $Cs_9(SmW_{10}O_{36})$ salt and $SmW_{10}O_{36}$–LDH, arises

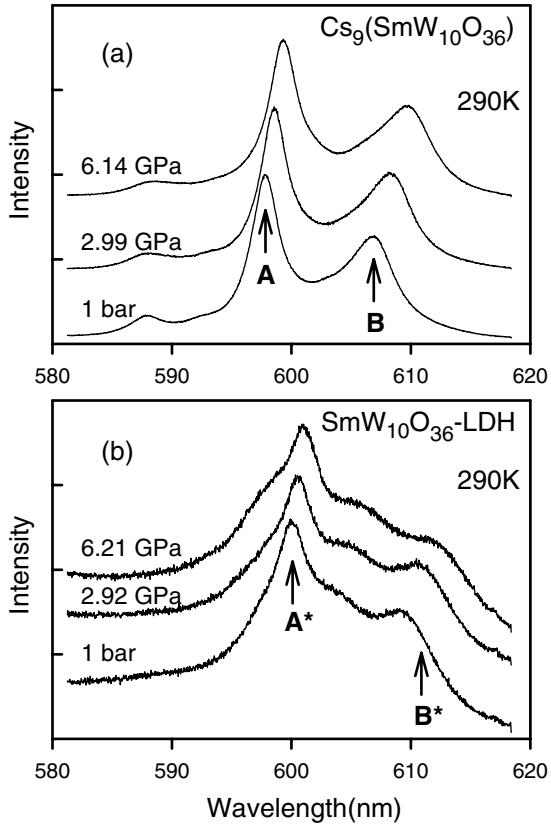


**Figure 4.** Pressure dependence of the room temperature PL of (a) $Cs_9(SmW_{10}O_{36})$ and (b) $SmW_{10}O_{36}$–LDH. For the sake of clarity, the lineshapes were normalized and displaced vertically by appropriate distances. In both cases (a) and (b), the peak positions redshift with increasing pressure.

purely from the deformation due to the uniaxial stress. This observation can be used to measure the uniaxial stress acting on the intercalants, when the external pressure is zero.

The position of A* varies linearly with increasing pressure. When the external pressure is zero, the position of peaks A and A* is 5978.9 and 6001.7 Å, respectively. If we divide the difference, (6001.7 − 5978.9) Å, by the pressure coefficient of peak A*, $\left(\frac{d\lambda}{dP}\right)_{A^*} = 1.63$ Å $GPa^{-1}$, then we find that the uniaxial stress $P_{eff}$ on the intercalants is given by

$$P_{eff} = (6001.7 - 5978.9)/1.63\,\text{GPa} \cong 13.9\,\text{GPa}.$$

In the discussion of figures 2 and 3, we pointed out that disappearance of many sharp peaks after intercalation implies that the host layers are exerting high pressure on the intercalating species. Our result is in accordance with this expectation.

The time evolution of PL at positions A of $Cs_9(SmW_{10}O_{36})$ salt and A* of $SmW_{10}O_{36}$–LDH also supports the previous observation. Figure 6(a) shows the time evolution of PL peak A at room temperature at several pressures. As can be seen in figure 6(a), the PL decay rate increases with increasing hydrostatic pressure. In figure 6(a), apart from the fast-decaying components appearing as sharp spikes around 2.984 $\mu$s, the PL at 1 bar has almost single-exponential decay with a lifetime of 102.6 $\mu$s. This long-time component (the decay after about 4.476 $\mu$s) is still single exponential at 3 GPa with lifetime of 64.4 $\mu$s. But at 5 GPa,

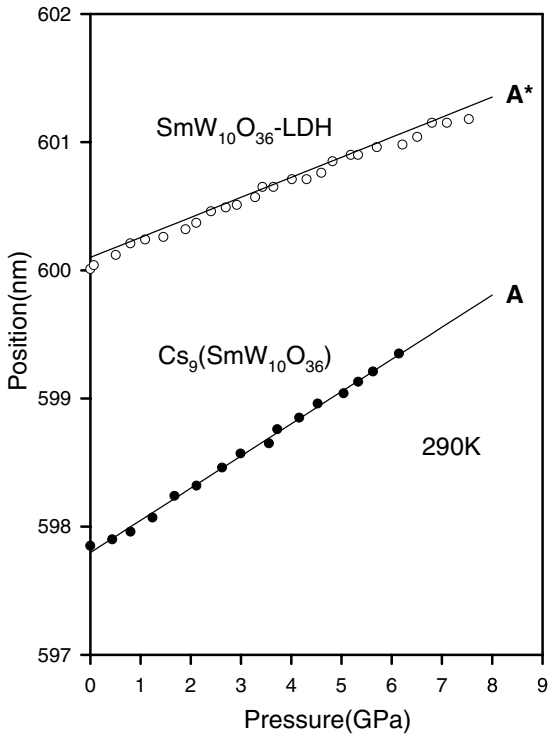


**Figure 5.** Pressure dependence of the peak positions A and A* at room temperature. Solid lines represent the fitting by straight lines. The difference in the slopes of the two cases is due to the difference between the effect generated by the hydrostatic presssure and the uniaxial stress.

it becomes a double-exponential decay (see the inset of figure 6(a)). Evidently, the overall effect pressure has on the long-time component of PL is to accelerate its decay. The inset of figure 6(a) displays the two lifetimes (long lifetime $T_L$ and short lifetime $T_S$) and the ratio of pre-exponential factors $A_S/A_L$ when the long-time component of PL was fitted with the form $A_L \exp(-t/T_L) + A_S \exp(-t/T_S)$.

Figure 6(b) shows decay curves of the peak A* from the intercalated compound. The decay curve of figure 6(b) even under ambient pressure is much faster than that under 6 GPa of the pre-intercalation compound ($Cs_9(SmW_{10}O_{36})$ salt) shown in figure 6(a). It is also well fitted with a bi-exponential decay form. Comparing figure 6(b) with 7(a), we see that the fast decay under ambient pressure is in good agreement with the fact that the intercalants are already under higher stress than 6 GPa, if we neglect the difference between the effects the uniaxial stress and the hydrostatic pressure generate. (Notice also that from figure 6(a), the PL has bi-exponential decay form at 5 GPa.) Other curves under higher pressures are also well fitted with bi-exponential decays and the fitting result is summarized in the inset of figure 6(b). The long lifetime increases with increasing pressure, but in both figures 6(a) and (b) the short-lifetime component increases with pressure ($A_S/A_L$ increases with pressure; see the insets).

### *3.2. Staging transformation*

Figure 7 displays the pressure dependence of the peak positions A and A* at four different temperatures. The pre-intercalation compound ($Cs_9(SmW_{10}O_{36})$ salt) shows only a small temperature-dependent variation of peak position at a given pressure. Also, their pressure

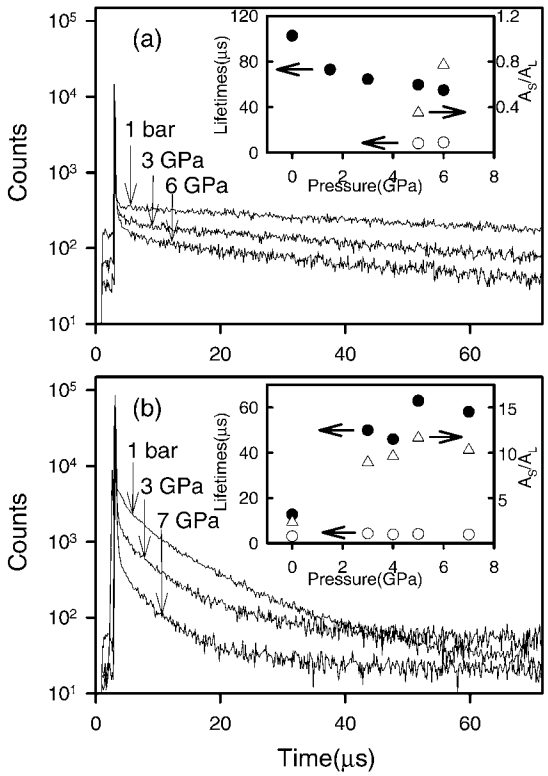


**Figure 6.** Time evolution of PL at peak position (a) A of pre-intercalation compound ($Cs_9(SmW_{10}O_{36})$ salt) and (b) A* of LDH intercalation compound under several pressures at room temperature. In the insets of (a) and (b) filled circles are long lifetimes $T_L$, empty circles short lifetimes $T_S$ and triangles the ratio $A_S/A_L$.

**Table 1.** Temperature-dependent pressure coefficients and the uniaxial stress.

| | 28 K | 120 K | 200 K | 290 K |
|---|---|---|---|---|
| $\left(\frac{d\lambda}{dP}\right)_A$ (Å $GPa^{-1}$) | $2.68 \pm 0.22$ | $2.65 \pm 0.09$ | $2.59 \pm 0.09$ | $2.88 \pm 0.17$ |
| $\left(\frac{d\lambda}{dP}\right)_{A^*}$ (Å $GPa^{-1}$) | $2.25 \pm 0.13$ | $2.01 \pm 0.11$ | $1.89 \pm 0.07$ | $1.63 \pm 0.16$ |
| Uniaxial stress $P_{eff}$ (GPa) | 7.6 | 9.5 | 10.7 | 13.9 |

coefficients of peaks at four different temperatures are almost identical (see table 1). In contrast, the peak positions of the intercalation compound are more sensitive to the temperature variation in the pressure range investigated. Moreover, the pressure coefficients are strongly temperature dependent (see table 1). From these data, we calculate the magnitude of uniaxial stress at four temperatures and the result is summarized in table 1. It is seen that the uniaxial stress varies significantly from 7.6 GPa at 28 K to 13.9 GPa at 290 K.

The temperature-dependent variation of the uniaxial stress by this large magnitude looks very unusual at first sight. However, this phenomenon can be well understood in terms of structural transformation, namely staging transformation. The staging phenomenon is characterized by a staging number $n$ which refers to the number of host layers separating

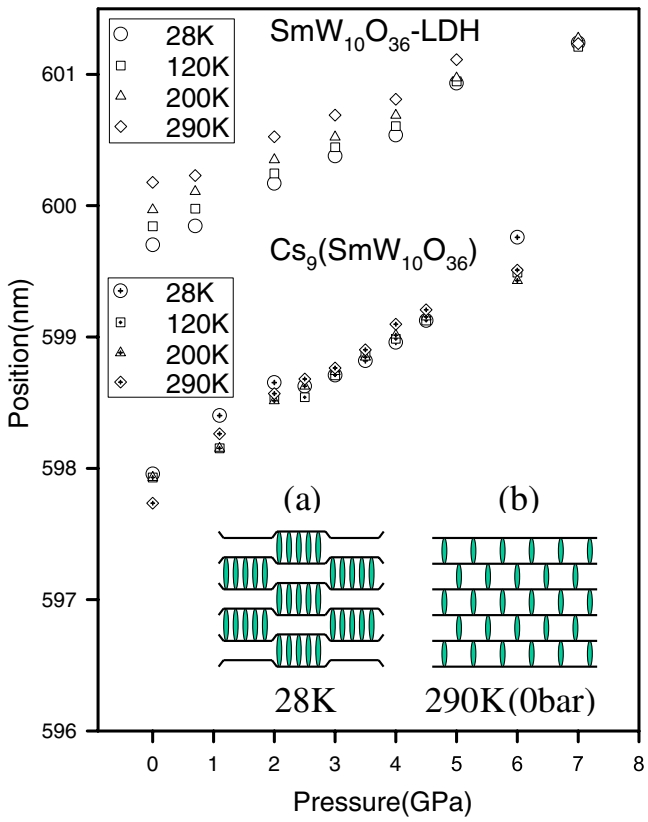


**Figure 7.** Pressure-dependent peak position A and A* at four temperatures. The pressure coefficients are strongly temperature dependent for $SmW_{10}O_{36}$–LDH, but almost identical for $Cs_9(SmW_{10}O_{36})$. Inset: (a) stage-2 configuration at 28 K and (b) stage-1 configuration at 290 K under ambient pressure. Horizontal lines represent host layers and each vertical object between the host layers represents a single intercalant. In inset (a) the intercalants appear longer in the *c*-axis direction to denote that they are under less stress than those in the stage-1 configuration shown in inset (b).

(This figure is in colour only in the electronic version)

two adjacent guest layers. Thus while a stage-1 compound has guest layers in every gallery space, not all the gallery spaces of stage-$n$ compounds for $n > 1$ are filled with guest ions. Due to the finite rigidity of the host layers, they pucker around the intercalating ions and this elastic deformation of the host layers causes elastic interaction between intercalants. The competition between the attractive intralayer elastic interaction and the repulsive interlayer elastic interaction is one of the main causes for the staging phenomena [5]. The host layers of the LDH are composed of three atomic layers, which allows them to have the flexibility intermediate between that of graphite and that of vermiculite. The host layer of graphite consists of a single atomic layer and that of vermiculite seven atomic layers. Accordingly, the former has great flexibility and is famous for its staging and the latter is very rigid and has only stage-1 compounds. We therefore expect that the LDH intercalation compound considered here will exhibit some staging phenomena.

At room temperature, the LDH intercalation compound is predominantly in stage-1 configuration as is evident with the XRD result. As the temperature is reduced, the elastic interaction

between the intercalants begins to overcome the thermal energy. The elastic interaction is attractive for the intercalants located in the same gallery and largely repulsive between the intercalants located in the different galleries. Thus at low temperatures, the intercalants in the same gallery will reduce their separations whose minimum value is determined by, for example, the repulsive Coulomb interaction between the intercalants. In addition to this in-plane structural re-ordering, the intercalants in the different layers will repel each other. In this case, macroscopic homogeneity is maintained only if the region of high density of intercalants and the region of low density appear alternately. Thus, islands of intercalants will be formed. Therefore, the configuration at low temperatures will be something similar to the example shown in inset (a) of figure 7 which schematically depicts a stage-2 compound at low temperature. At the lowest temperature it is also possible to have a stage-3 configuration or a mixture of various stages. Regardless of the exact stage configuration which is not readily available at the present stage, it is evident that the average degree of stage increases with decreasing temperature. For example, at the stage-2 configuration shown in inset (a) of figure 7, it is obvious that uniaxial stress of the host layers acting on the intercalants is mitigated from that of the stage-1 configuration at high temperature shown in the inset (b). This is because there are now no intercalants in the consecutive galleries and the host layers have room for relaxation.

We now consider the pressure coefficients of the peak position versus temperature. From table 1 we see that $\left(\frac{\mathrm{d}\lambda}{\mathrm{d}P}\right)_{A^*}$ of the intercalation compound decreases from $2.25 \pm 0.13$ Å GPa$^{-1}$ at 28 K to $1.63 \pm 0.16$ Å GPa$^{-1}$ at 290 K while $\left(\frac{\mathrm{d}\lambda}{\mathrm{d}P}\right)_{A}$ of the pre-intercalation compound ($Cs_9(SmW_{10}O_{36})$ salt) is nearly temperature independent. This temperature variation of $\left(\frac{\mathrm{d}\lambda}{\mathrm{d}P}\right)_{A^*}$ can be understood in terms of pressure-driven staging transformation. In the work of [19] it was shown that high pressure induces a staging transition from stage 2 to stage 3 for the graphite intercalation compound $KC_{24}$. This effect arises because pressure increases the local deformation of the host layers around the intercalants, promoting the elastic interactions between the intercalants. At 28 K, a large portion of the LDH-intercalation compound is already in a higher-staged configuration like the one shown in inset (a) of figure 7, even at 0 bar. Therefore, increasing the pressure at 28 K will not change the stage configuration much. Accordingly, the effect of external pressure at low temperatures is mainly to deform the intercalants. In contrast, consider now the case of room temperature. Since a large portion of the sample is in the stage-1 configuration at 0 bar, applying external pressure will cause the transition into a higher-staged configuration. Actually, it is very likely that the various stages coexist under high pressure. However, the average degree of stage would increase with increasing pressure. The external pressure at room temperature not only deforms the intercalants but also increases the average stage number. Therefore, for a given pressure increment, the intercalants at 290 K are less deformed than the case of 28 K since they find increased room for relaxation at increased pressure, which explains our observation.

In addition to the stage-transformation process mentioned above, it could be contemplated that the stage-transformation occurs as a result of partial de-intercalation. However, such de-intercalation breaks the overall charge neutrality of the sample. Moreover, after releasing the pressure the PL returned to its original state. Similarly, cycling the temperature did not entail any hysteresis with the PL. All these indicate that the stage-transformation process induced by the de-intercalation is not a feasible process.

## 4. Conclusion

An LDH intercalation compound with Sm ion complex as intercalant was synthesized. We measured the uniaxial stress the host layers of the LDH intercalation compound exert on the Sm ion complex intercalants. The PL of the Sm ion complex was employed to measure

the uniaxial stress because it was sensitive to the surroundings. To find the uniaxial stress, hydrostatic pressure was applied to the intercalation compound and the resulting redshift of the PL versus pressure was measured. The magnitude of the redshift varied linearly with pressure. We then compared the peak positions of the PL before and after the intercalation and divided the difference by the redshifting rate. The time evolution of PL of both samples was also dependent on the pressure and it strongly supported the observation that the Sm ion complexes were under large uniaxial stress even in the absence of external pressure. The temperature dependence was also measured and the uniaxial stress revealed great variation in the temperature range between 28 and 290 K. It was shown that this great variation of the uniaxial stress versus temperature implies the staging transformation to a higher degree as the temperature is lowered. The slowdown of the deformation of the intercalants at higher temperatures was explained in terms of the pressure-induced staging transition.

Theoretical calculation of the uniaxial stress would be primarily based upon the Coulomb interaction between the host layers and the Sm ion complexes. However, such calculation is difficult to perform due to the lack of knowledge of charge distribution in the host layer. Thus the experimental result presented in this paper corresponds to a case where it is difficult to obtain the theoretical one.

## Acknowledgment

This work was supported by the Basic Research Program of the Korea Science and Engineering Foundation under grant no 2000-1-11400-005-2 (R02-2000-00049).

## References

[1] Solin S A 1982 *Adv. Chem. Phys.* **49** 455
[2] Solin S A 1984 *J. Mol. Catal.* **27** 293
[3] Grim R E 1968 *Clay Mineralogy* 2nd edn (New York: McGraw-Hill)
[4] Reichle W T 1986 *Solid State Ion.* **22** 135
[5] Safran S A 1987 *Solid State Phys.* **40** 183
[6] Alberti G and Bein T (ed) 1996 *Comprehensive Supramolecular Chemistry* vol 7 (Amsterdam: Elsevier)
[7] Caswell N, Solin S A, Hayes T M and Hunter S J 1980 *Physica* B **99** 463
[8] Mori M, Moss S C, Yan Y M and Zabel H 1982 *Phys. Rev.* B **25** 1287
[9] Park T and Lee S 1996 *Solid State Commun.* **100** 257
[10] Park T 1998 *Solid State Commun.* **108** 523
[11] Kirczenow G 1982 *Phys. Rev. Lett.* **49** 1853
[12] Millman S E and Kirczenow G 1983 *Phys. Rev.* B **28** 3482
[13] Dahn J R, Dahn D C and Haering R R 1982 *Solid State Commun.* **42** 179
[14] Kim H, Jin W, Lee S, Zhou P, Pinnavaia T J, Mahanti S D and Solin S A 1988 *Phys. Rev. Lett.* **60** 2168
[15] Thorpe M F 1989 *Phys. Rev.* B **39** 10370
[16] Solin S A, Lee S, Miyazaki H and Mahanti S D 1989 *Synth. Met.* **34** 243
[17] Lee S, Miyazaki H, Mahanti S D and Solin S A 1989 *Phys. Rev. Lett.* **62** 3066
[18] Thorpe M F, Jin W and Mahanti S D 1989 *Phys. Rev.* B **40** 10294
[19] Clarke R, Wada N and Solin S A 1980 *Phys. Rev. Lett.* **44** 1616
[20] Holtz M, Park T, Amerasekera J, Solin S A and Pinnavaia T J 1994 *J. Chem. Phys.* **100** 3346
[21] Park T, Lee S, Holtz M and Solin S A 1995 *Phys. Rev.* B **51** 17925
[22] See, for example,
O'Connor D V and Phillips D 1984 *Time-Correlated Single Photon Counting* (London: Academic)
[23] Piermarini G J, Block S, Barnett J D and Forman R A 1975 *J. Appl. Phys.* **46** 2779
[24] Peacock R D and Weakly T J R 1971 *J. Chem. Soc.* A 1836
[25] Park T, Park T Y and Kim H 2000 *Sae Mulli* **40** 218
[26] Iball J, Low N J and Weakley T J R 1974 *J. Chem. Soc. Dalton Trans.* 2021
[27] Yamashita N and Asano S 1987 *J. Phys. Soc. Japan* **56** 352
[28] Yoo C S, Radousky H B and Holmes N C 1991 *Phys. Rev.* B **44** 830